Since January 2020 Elsevier has created a COVID-19 resource centre with free information in English and Mandarin on the novel coronavirus COVID-19. The COVID-19 resource centre is hosted on Elsevier Connect, the company's public news and information website.

Available online at www.sciencedirect.com
ScienceDirect
Virology 360 (2007) 264–274
VIROLOGY
www.elsevier.com/locate/yviro

Palmitoylation of the cysteine-rich endodomain of the SARS–coronavirus spike glycoprotein is important for spike-mediated cell fusion

Chad M. Petit [a,b], Vladimir N. Chouljenko [a,b], Arun Iyer [a,b], Robin Colgrove [c], Michael Farzan [d], David M. Knipe [c], K.G. Kousoulas [a,b,*]

[a] Division of Biotechnology and Molecular Medicine (BIOMMED), USA
[b] Department of Pathobiological Sciences, School of Veterinary Medicine, Louisiana State University, Baton Rouge, LA 70803, USA
[c] Department of Microbiology and Molecular Genetics, Harvard Medical School, Boston, MA 02115, USA
[d] Partners AIDS Research Center, Brigham and Women's Hospital, Department of Medicine (Microbiology and Molecular Genetics), Harvard Medical School, Boston, MA 02115, USA

Received 23 June 2006; returned to author for revision 14 August 2006; accepted 18 October 2006
Available online 28 November 2006

Abstract

The SARS–coronavirus (SARS–CoV) is the etiological agent of the severe acute respiratory syndrome (SARS). The SARS–CoV spike (S) glycoprotein mediates membrane fusion events during virus entry and virus-induced cell-to-cell fusion. The cytoplasmic portion of the S glycoprotein contains four cysteine-rich amino acid clusters. Individual cysteine clusters were altered via cysteine-to-alanine amino acid replacement and the modified S glycoproteins were tested for their transport to cell-surfaces and ability to cause cell fusion in transient transfection assays. Mutagenesis of the cysteine cluster I, located immediately proximal to the predicted transmembrane, domain did not appreciably reduce cell-surface expression, although S-mediated cell fusion was reduced by more than 50% in comparison to the wild-type S. Similarly, mutagenesis of the cysteine cluster II located adjacent to cluster I reduced S-mediated cell fusion by more than 60% compared to the wild-type S, while cell-surface expression was reduced by less than 20%. Mutagenesis of cysteine clusters III and IV did not appreciably affect S cell-surface expression or S-mediated cell fusion. The wild-type S was palmitoylated as evidenced by the efficient incorporation of ^{3}H-palmitic acid in wild-type S molecules. S glycoprotein palmitoylation was significantly reduced for mutant glycoproteins having cluster I and II cysteine changes, but was largely unaffected for cysteine cluster III and IV mutants. These results show that the S cytoplasmic domain is palmitoylated and that palmitoylation of the membrane proximal cysteine clusters I and II may be important for S-mediated cell fusion.

Keywords: SARS; Coronavirus; Spike; Cysteine-rich; Fusion

Introduction

An outbreak of atypical pneumonia, termed severe acute respiratory syndrome (SARS), appeared in the Guangdong Province of southern China in November, 2002. The mortality rates of the disease reached as high as 15% in some age groups (Anand et al., 2003). The etiological agent was found to be a novel coronavirus, which was named the SARS–coronavirus (SARS–CoV) (Drosten et al., 2003; Ksiazek et al., 2003; Peiris et al., 2003). Analysis of the viral genome has demonstrated that the SARS–CoV is phylogenetically divergent from the three known antigenic groups of coronaviruses (Drosten et al., 2003; Ksiazek et al., 2003). However, analysis of the polymerase gene alone, indicated that the SARS–CoV may be an early offshoot from the group 2 coronaviruses (Snijder et al., 2003).

The coronaviruses are the largest of the enveloped RNA viruses with a positive-stranded RNA genome of 28 to 32 kb (Holmes, 2003). Coronaviruses possess a wide host range, capable of infecting mammalian and avian species. All identified coronaviruses have a common group of indispensable genes that encode nonstructural proteins including the RNA

* Corresponding author. Department of Pathobiological Sciences, School of Veterinary Medicine, Louisiana State University, Baton Rouge, LA 70803, USA.
E-mail address: vtgusk@lsu.edu (K.G. Kousoulas).

0042-6822/$ - see front matter © 2006 Elsevier Inc. All rights reserved.
doi:10.1016/j.virol.2006.10.034

replicase gene open reading frame (ORF) 1ab and the structural proteins nucleocapsid (N), membrane protein (M), envelope protein (E), and spike glycoprotein (S), which are assembled into virus particles. A hemagglutinin–esterase (HE) protein is also encoded by some coronaviruses. Dispersed among the major viral genes are a series of ORFs that are specific to the different coronavirus groups. Functions of the majority of these ORFs have not been determined.

The SARS spike glycoprotein, a 1255-amino-acid type I membrane glycoprotein (Rota et al., 2003), is the major protein present in the viral membrane forming the typical spike structure found on all coronavirions. The S glycoprotein is primarily responsible for entry of all coronaviruses into susceptible cells through binding to specific receptors on cells and facilitating subsequent virus–cell fusion (Cavanagh, 1995). The S glycoprotein specified by mouse hepatitis virus (MHV) is cleaved into S1 and S2 subunits, although cleavage is not necessarily required for virus–cell fusion (Bos et al., 1997; Gombold et al., 1993; Stauber et al., 1993). Similarly, the SARS–CoV S glycoprotein may be cleaved into S1 and S2 subunits in Vero E6-infected cells (Wu et al., 2004), while it is not known whether this cleavage affects S-mediated cell fusion. The SARS–CoV receptor was identified as the angiotensin-converting enzyme 2 (ACE2) (Li et al., 2003).

Although the exact mechanism by which the SARS–CoV enters the host cell has not been elucidated, it is most likely similar to mechanisms proposed for other coronaviruses. Generally, upon receptor binding at the cell membrane, the S glycoprotein is thought to undergo a dramatic conformational change causing exposure of a hydrophobic fusion peptide, which is subsequently inserted into cellular membranes. This conformational change of the S glycoprotein causes close apposition of viral and cellular membranes followed by membrane fusion resulting in entry of the virion nucleocapsids into cells (Eckert and Kim, 2001; Tsai et al., 2003; Zelus et al., 2003). This series of S-mediated virus entry events is similar to other class I virus fusion proteins (Baker et al., 1999; Melikyan et al., 2000; Russell et al., 2001).

Important structural elements of the S ectodomains required for stabilization of conformational structures of S immediately preceding membrane fusion are the heptad repeat (HR) amino acid regions (Fig. 1). The HRs contain a sequence motif characteristic of coiled-coils, which appear to be a common motif in many viral and cellular fusion proteins (Skehel and Wiley, 1998). These coiled-coil regions allow the protein to fold back upon itself as a prerequisite step to initiating the membrane fusion event. There are usually two HR regions: an N terminal HR region adjacent to the fusion peptide and a C-terminal HR region close to the transmembrane domain (TMD) of the protein (Fig. 1).

Based on structural similarities, two classes of viral fusion proteins have been established (Kielian, 2006; Lescar et al., 2001). Class I viral fusion proteins, such as the SARS–CoV S glycoprotein contain two heptad repeat regions and an N-terminal or N-proximal fusion peptide (Fig. 1). Class II viral fusion proteins lack heptad repeat regions and contain an internal fusion peptide (Lescar et al., 2001). Typically, the ectodomains of the S2 subunits of coronaviruses contain two heptad regions, HR1 and HR2 located proximal to the transmembrane region (de Groot et al., 1987) (Fig. 1). These HRs form a six-helix bundle having three α-helices formed by HR1 and three antiparallel HR2 α-helices. Formation of this six-helix bundle brings the fusion peptide in close proximity to the TMD of the S glycoprotein, a prerequisite step to membrane fusion (Bosch et al., 2003). Although the structure of the HR1–HR2 complex has been solved in peptide reconstitution experiments (Ingallinella et al., 2004), the conformational changes that result in the six-helix bundle are not known. Presumably, S binding to cellular receptor and/or activation by low-pH conditions initiates the cascade of conformational events that result in the six-helix bundle, which is ultimately stabilized by the HR affinities for each other. The fusion peptide of the coronavirus S glycoprotein is predicted to be at the N-terminus of S2 (Sainz et al., 2005).

The carboxyl termini of certain viral class I fusion proteins have been shown to play regulatory roles in membrane fusion (Bagai and Lamb, 1996; Gabuzda et al., 1992; Sergel and Morrison, 1995; Seth et al., 2003; Tong et al., 2002; Yao and Compans, 1995). Specifically for coronaviruses, the MHV S glycoprotein carboxyl terminus was shown to contain cysteine-rich regions, which were critical for fusion of infected cells (Bos et al., 1995; Chang et al., 2000; Ye et al., 2004). The SARS–CoV S glycoprotein has relatively high (3%) cysteine content (39 residues). Nine of the cysteine resides are concentrated in a region that spans the putative TMD and the cytoplasmic domain, with six of these residues being well conserved among different coronaviruses (Fig. 1). The precise boundaries of the S TMD specified by different coronaviruses are not known, and different predictions include or exclude part of the cysteine-rich domain as part of the TMD (Broer et al., 2006; Chang et al., 2000; Godeke et al., 2000; Ye et al., 2004). Inclusion of part of the cysteine-rich motif produces a TMD of 34 amino acids, which is longer than necessary to cross the membrane (Broer et al., 2006).

Regardless of the native location of the cysteine residues in either the TMD or the cytoplasmic portions of S, this unusual concentration and conservation of cysteine among all coronaviruses suggests that they play an important role in S glycoprotein function. For MHV, studies have shown that the cysteine rich domain is required for coronavirus-induced membrane fusion. Specifically, substitution of the cytoplasmic portion of the cysteine-rich region including the cytoplasmic tail of MHV S with the cytoplasmic tail of the VSV-G protein abolished MHV S glycoprotein-mediated cell–cell fusion (Bos et al., 1995). Other studies showed that while the cysteine-rich domain was not the sole functional domain of the transmembrane anchor required for fusion activity, it was apparently necessary for fusion activity (Chang et al., 2000).

In this study, cysteine-to-alanine mutagenesis was used to elucidate which cysteine clusters were dispensable for protein transport and SARS–CoV S-mediated cell–cell fusion. Cysteine-rich domains that are immediately proximal to the intramembrane sequence of S were found to be important for S-mediated cell fusion. In addition, S was shown to be

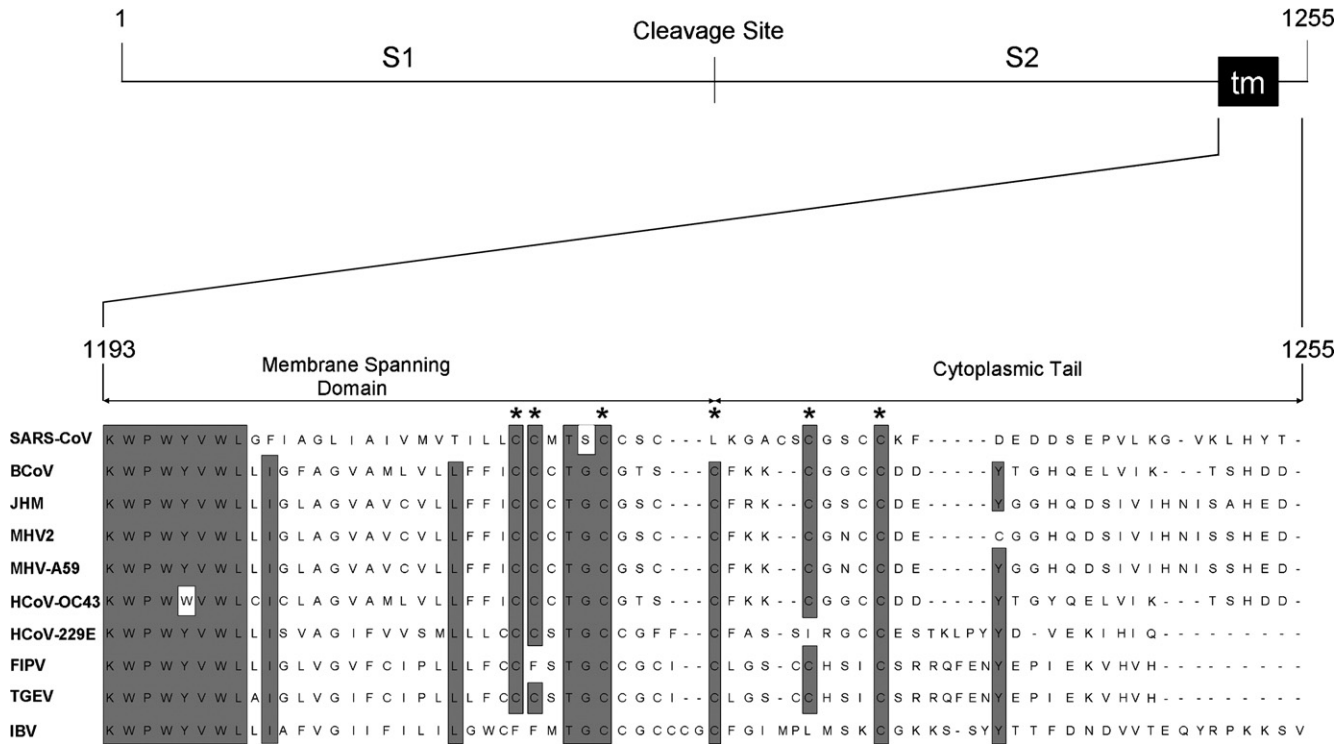

Fig. 1. Alignment of the membrane spanning domain and endodomain of the spike glycoprotein from ten different coronaviruses. A schematic diagram of the SARS–CoV S protein from amino acid 1 to amino acid 1255 is shown at the top of the figure. A vertical line demarcates the potential cleavage between the S1 and S2 subunits of the protein. The carboxyl terminus (amino acids 1193 to 1255) of the SARS–CoV S glycoprotein is shown enlarged below aligned with the same region of the S glycoprotein specified by other coronaviruses. Viruses from antigenic group I (feline infectious peritonitis virus [FIPV], transmissible gastroenteritis virus [TGEV′, human coronavirus 229E [HCoV–229E]), antigenic group II (three different mouse hepatitis virus strains [A59, JHM, and MHV2], bovine coronavirus [BCoV], and human coronavirus OC43 [HCoV–OC43]), and antigenic group III (infectious bronchitis virus [IBV]) are represented in the alignment. The membrane spanning domain and the cytoplasmic tail are denoted with arrows above the alignment. Residues conserved in at least eight of the ten coronaviruses represented are indicated by the shaded residues. Cysteines that are highly conserved throughout all of the S proteins are noted by asterisks (Abraham et al., 1990; Binns et al., 1985; Delmas et al., 1992; Kunkel and Herrler, 1993; Luytjes et al., 1987; Marra et al., 2003; Mounir and Talbot, 1993; Parker et al., 1989; Raabe et al., 1990; Rasschaert and Laude, 1987).

palmitoylated at these cysteine-rich domains suggesting that S carboxyl terminal palmitoylation may be important for its fusogenic properties. These results are in general agreement with previous findings with other coronaviruses, most notably MHV (Bos et al., 1995; Chang et al., 2000).

Results

Genetic analysis of the S glycoprotein cysteine-rich domain

The exact limits of the SARS S transmembrane region are not known. Predictions cited in the literature for different coronaviruses place part of the cysteine-rich carboxyl terminal motif within the TMD(Broer et al., 2006). The Web-based algorithm Prediction of Transmembrane Regions and Orientation (TMPpred), predicts amino acid residues 1198–1215 (VWLGFIAGLIAIVMVTILL) as a strongly preferred model TMD and the sequence 1199–1219 (LGFIAGLIAIVMVTILLCCM) as an alternative model TMD. In contrast, the Classification and Secondary Structure Prediction of Membrane Proteins (SOSUI) WEB-based algorithm (Hirokawa et al., 1998) predicts the amino acid residues 1201–1223 (GFIAGLIAIVMVTILLCCMTSCC) as a potential TMD. For presentation and discussion purposes as well as for reasons that will become apparent in the discussion section of this paper, we have chosen to represent the TMD as predicted by TMPpred, which places the entire cysteine-rich motif as part of the S endodomain (Figs. 1 and 2). In a recent manuscript, we referred to the cysteine-rich regions as cysteine clusters CRM1 and CRM2 (Petit et al., 2005). In this work, we have further subdivided CRM1 into cysteine clusters CL-I and CL-II, and CRM2 into cysteine clusters CL-III and CL-IV (Fig. 2). To elucidate the role of the S carboxyl terminal cysteine-rich domains in membrane fusion, intracellular transport, and cell surface expression, mutated S genes carrying cysteine cluster-to-alanine mutations were constructed by replacing all cysteine residues within the CL-I, CL-II, CL-III or CL-IV positions generating S mutant genes mCL-I, mCL-II, mCL-III and mCL-IV, respectively (Fig. 2).

Effects of mutations on S synthesis

Western immunoblot analysis was used to detect expression of all constructed mutant glycoproteins as well as the wild-type after transfection of Vero cells (Fig. 3). Cellular lysates prepared from transfected cells at 48 h post-transfection were electrophoretically separated by SDS–PAGE and the S glycoproteins were detected via chemiluminescence using a monoclonal antibody specific for the S1 portion of the SARS–CoV S

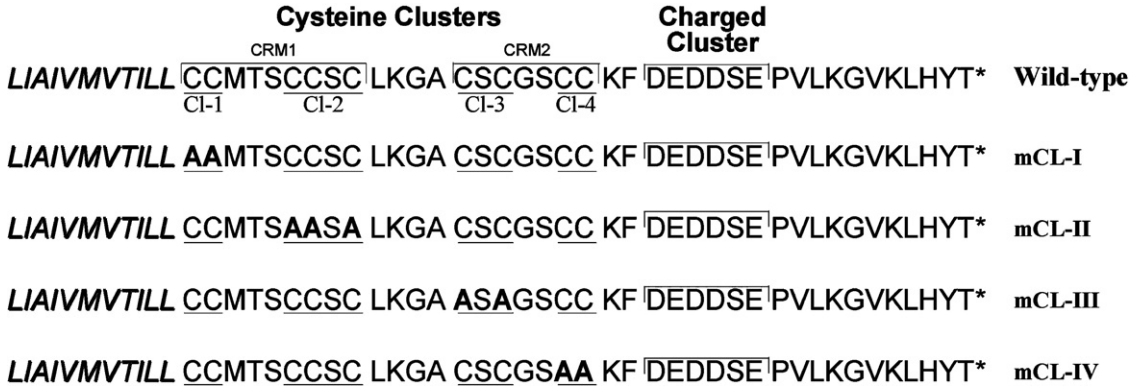

Fig. 2. Schematic diagram of the SARS–CoV S glycoprotein endodomain and the cysteine cluster to alanine mutations. Amino acid sequences of the carboxyl termini and the cysteine cluster-to-alanine mutations are shown for the wild-type as well as the mutant proteins. The cysteine clusters (CRM1 and CRM2) and the charged rich regions of the S proteins are encompassed in brackets and labeled. The transmembrane portion of the endodomain is italicized and underlined. Amino acids mutated to alanines for the mCL-I, mCL-II, mCL-III, and mCL-IV cluster mutations are in bold.

glycoprotein as we have recently described (Petit et al., 2005). Carbohydrate addition was shown to occur in at least four different locations of the SARS–CoV S glycoprotein (Krokhin et al., 2003; Ying et al., 2004). Furthermore, transiently expressed S glycoprotein in Vero E6 cells can be proteolytically cleaved into S1 and S2 components (Wu et al., 2004). The anti-S monoclonal antibody SW-111 detected a protein species in cellular extracts from transfected cells, which migrated with an apparent molecular mass of approximately 180 kDa, as reported previously (Song et al., 2004). All mutated S glycoproteins produced similar S-related protein species in comparison with the wild-type S indicating that none of the engineered mutations adversely affected S synthesis and intracellular processing (Fig. 3). Similar results were obtained when the mCL-I and mCL-II mutations were combined into the S mutant form mCL-I+II (not shown).

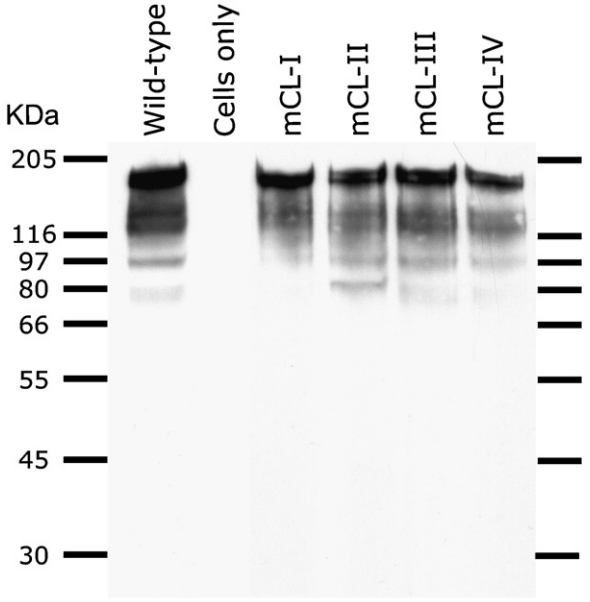

Fig. 3. Western blot analysis of the expressed mutant SARS–CoV mutant glycoproteins. Immunoblots of wild-type [So–3xF(WT)] and cysteine to alanine mutant S glycoproteins probed with monoclonal anti-SARS S antiserum. "Cells only" represents a negative control in which mock-transfected Vero cells were probed with the monoclonal antibody to the SARS–CoV S glycoprotein.

Ability of mutant S glycoproteins to be expressed on the cell surface

Immunohistochemical analysis was used to label cell-surface expressed S under live cell conditions, and to determine total S expression after fixing and permeabilizing the cells prior to reaction (Fig. 4). An ELISA was used to quantitatively determine the relative amounts of cell-surface and total cellular expressed S glycoprotein. A ratio between the cell-surface localized S and total cellular S expressed was then calculated and normalized to the corresponding ratio obtained with the wild-type S glycoprotein (see Materials and methods) (Fig. 5). All cysteine cluster to alanine mutants were expressed on the cell surface at rate comparable to that of the wild-type. Specifically, the levels of each S mutant expression on the transfected cell surfaces in comparison to the wild-type S were: mCL-I (91%), mCL-II (87%), mCL-III (101%), and mCL-IV (110%). The S mutant form mCL-I+II expressed on transfected cell surfaces at approximately 95% of the wild-type S (not shown).

Effects of mutations on the palmitoylation of the S glycoprotein

The carboxyl terminal cysteine residues of the MHV S have been shown to be palmitoylated (Bos et al., 1995). To determine if the SARS S was also palmitoylated , transiently expressed wild-type S and mutant forms containing cysteine-to-alanine substitutions were assayed for their ability to incorporate [^{3}H] palmitic acid. After labeling, the cellular lysates were electrophoretically separated by SDS–PAGE and visualized by fluorography (see Materials and methods) (Fig. 6A). The wild-type S produced a protein species at the expected apparent molecular mass of 180 kDa, which indicates that the SARS–CoV S is palmytoylated. Similarly, each S mutant produced an S-related protein species with the expected molecular mass of full-size S. However, only the mCL-IV mutant appeared to be palmitoylated as well as the wild-type S (Fig. 6A). To determine the relative level of S palmitoylation, all S protein species film

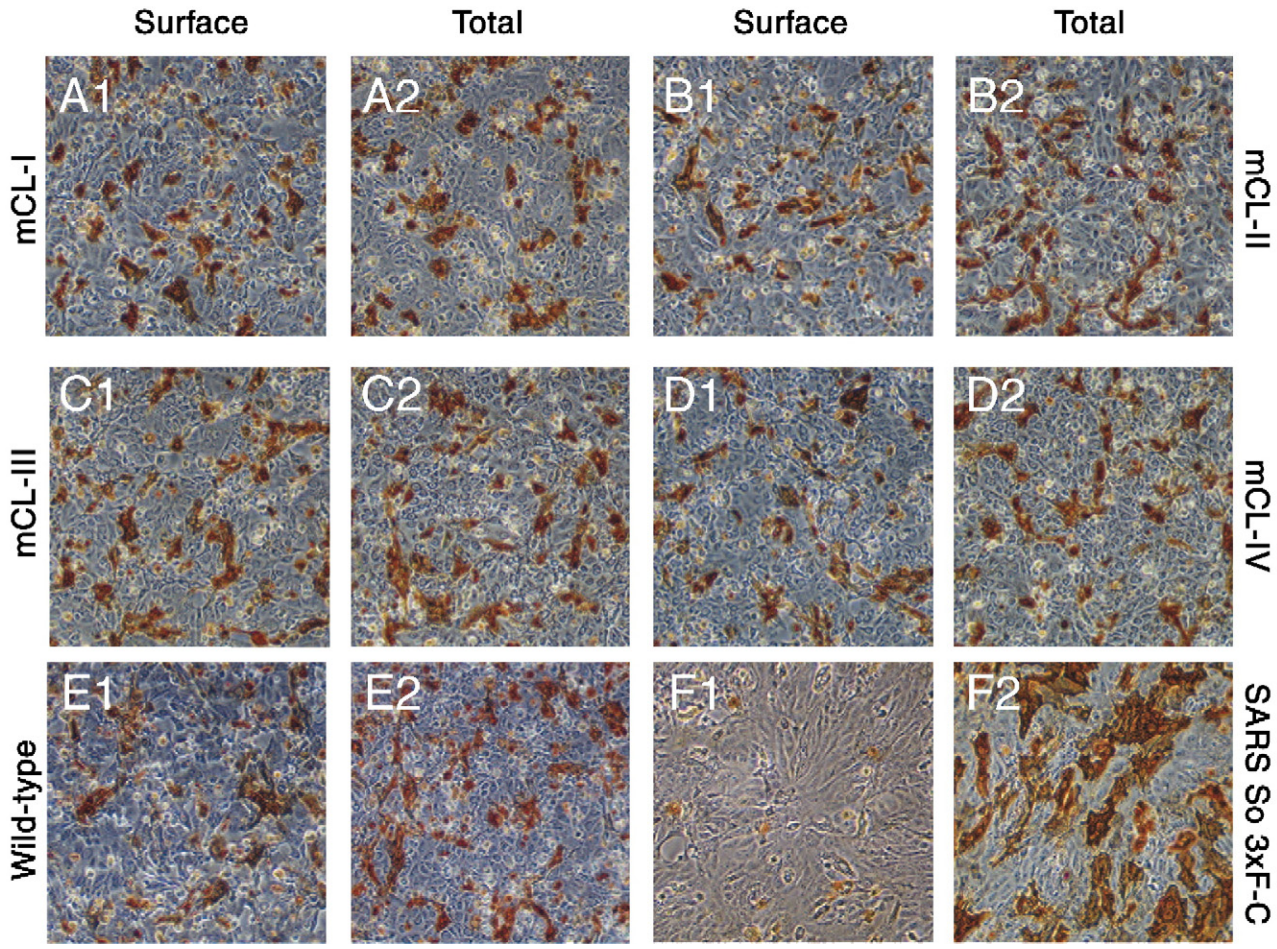

Fig. 4. Immunohistochemical detection of cell-surface and total expression of the SARS–CoV S wild-type and mutant proteins. Vero cells were transfected with the wild-type SARS–CoV optimized S (SARS So 3xF) (E1, E2), mCL-I (A1, A2), mCL-II (B1, B2), mCL-III (C1, C2), mCL-IV (D1, D2), and a wild-type SARS–CoV optimized S labeled with a 3xFLAG carboxyl tag (F1, F2), which served as a negative control. At 48 h post-transfection, cells were immunohistochemically processed under live conditions to detect cell-surface expression (A1, B1, C1, D1, E1, and F1), or permeabilized conditions to detect total expression (A2, B2, C2, D2, E2, and F2) using the anti-FLAG antibody.

images obtained by autoradiography were scanned, digitally analyzed, and normalized to the total protein of the sample obtained by spectrophotometry (not shown). The amount of palmitoylation was then expressed as a ratio to the relative amount of wild-type S (see Materials and methods). Palmitoylation of the mCL-I and mCL-II mutants was reduced by 56% and 49%, respectively. Palmitoylation of the mCL-III mutant was at similar levels to the wild-type S while palmitoylation of the mCL-IV mutant was reduced by approximately 5%. (Fig. 6B).

To further assess the contribution of the mCL-I and mCL-II mutations in the observed inhibition of S palmitoylation, a mutant S form was constructed carrying both the mCL-I and mCL-II mutations. Palmitoylation experiments revealed that palmitoylation of the mCL-I+II S mutant form was reduced by approximately 80% in comparison to the wild-type S (Figs. 7A, B).

Effects of mutations on S-mediated cell-to-cell fusion

Transiently expressed wild-type S causes extensive cell-to-cell fusion (syncytial formation), especially in the presence of the SARS–CoV ACE2 receptor (Li et al., 2003; Petit et al., 2005) To determine the ability of each cysteine cluster to alanine mutant S glycoprotein to cause cell-to-cell fusion and the formation of syncytia, fused cells were labeled by immunohistochemistry using the anti-FLAG antibody. The extent of cell-to-cell fusion caused by each mutant glycoprotein was then calculated by obtaining the average size of approximately 300 syncytia (Fig. 8). Typically, all transfections produced a similar number of syncytia (not shown). The average syncytium size for each mutant was then normalized to that found in wild-type S transfected cells as outlined in the Materials and methods and detailed previously (Petit et al., 2005). The mCL-I (54%), mCL-II (62%), mCL-III (15%), and mCL-IV (14%) mutants inhibited the formation of syncytia by the percentages indicated (Fig. 8).

Discussion

Previous studies have shown that the intracytoplasmic endodomains of class I membrane proteins play an important role in intracellular transport and virus-induced cell-to-cell fusion (Bagai and Lamb, 1996; Bos et al., 1995; Chang et al.,

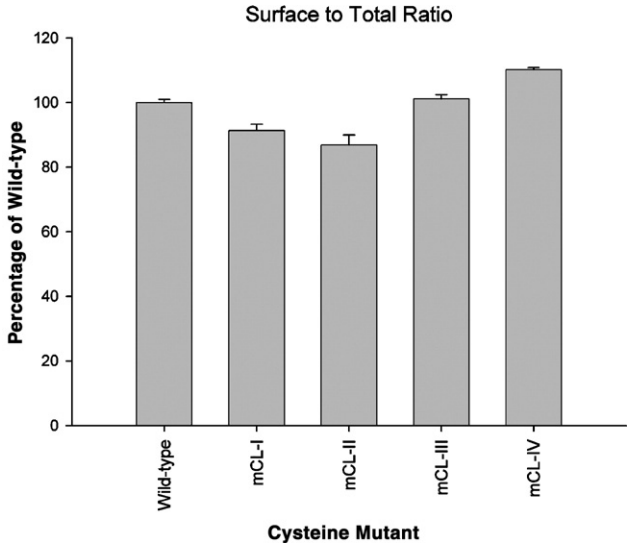

Fig. 5. Ratios of cell-surface to total cellular expression of mutant SARS–CoV S glycoproteins. Detection of cell surface and total glycoprotein distribution was determined by immunohistochemistry and ELISA (see Materials and methods). Cell-surface and total cell expression of the S glycoprotein was measured by immunohistochemistry. For cell-surface expression the transfected cell monolayers were reacted with anti-FLAG antibody at room temperature under live conditions. For total S glycoprotein detection, cells were fixed and permeabilized prior to reaction with the anti-FLAG antibody. A ratio between the amount of S detected on cell-surfaces to total cellular expression of S was calculated and normalized to the wild-type protein, and expressed as a percentage ratio of the wild-type S. The error bars represent the maximum and minimum surface to total ratios obtained from three independent experiments, and the bar height represents the average surface to total ratio as a percentage of the wild-type.

2000; Lontok et al., 2004; Petit et al., 2005; Schwegmann-Wessels et al., 2004; Sergel and Morrison, 1995; Tong et al., 2002; Waning et al., 2004; Yao and Compans, 1995). Recently, we reported that the endodomain of the SARS S glycoprotein contains distinct domains that function in intracellular transport, cell-surface expression and cell fusion (Petit et al., 2005). These results suggested the involvement of cysteine-rich motifs located in the carboxyl terminus of the SARS S in S-mediated cell fusion. In this study, we have analyzed via site-directed mutagenesis the relative contribution of each sub-cluster of cysteine residues in S synthesis, cell surface expression and S-mediated cell fusion. The salient features of our findings are: 1) Cysteine residues that are proximal to the TMD play crucial roles in S-mediated cell fusion; 2) The SARS-S is palmitoylated, most likely, at the two TMD-proximal cysteine sub-clusters. This work suggests that palmitoylation of the cytoplasmic terminus of the SARS S is important in S-mediated cell fusion.

Contribution of carboxyl terminal cysteine residues in S synthesis and S-mediated cell fusion

The mCL-I and mCL-II mutations are cysteine-to-alanine cluster mutations that target the two cysteine rich clusters most proximal to the transmembrane region of the S glycoprotein. Both of these S mutants were expressed on the cell surface at levels comparable to that of the wild-type (91% and 87%, respectively). However, S-mediated cell fusion was drastically reduced in comparison to the wild-type S. Specifically, cell fusion produced by the mCL-I and mCL-II cluster S mutants was reduced by 55% and 60%, respectively. Similar modifications of cysteine residues within the carboxyl terminus of the MHV S that correspond to the SARS S cysteine residues reduced MHV S-mediated cell fusion by 56% and 94%, respectively (Chang et al., 2000), indicating that these cysteine residues play important roles in both SARS–CoV and MHV S-mediated cell fusion.

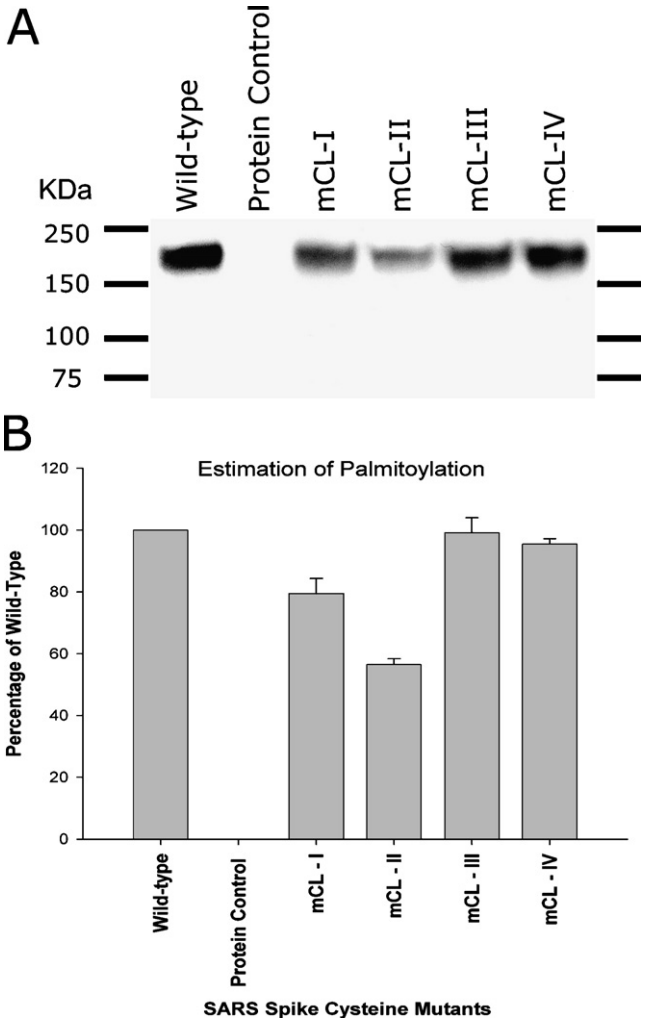

Fig. 6. Incorporation of [^{3}H] palmitic acid into wild-type and single cysteine mutant forms mCL-I, mCL-II, mCL-III and mCL-IV of the SARS–CoV S glycoprotein. (A) Autoradiographic images of immunoprecipitates resolved by SDS–PAGE electrophoresis of cellular extracts obtained from transfected Vero cells labeled with [^{3}H] palmitic acid. Apparent molecular mass controls are as shown. Sample from mock-transfected Vero cells was used as a negative protein control (protein control). The samples from transfected Vero cells with the wild-type {So–3xF (WT)} and each of the four mutated S genes are shown. (B) An estimation of the relative concentration of the palmitoylated S species in comparison to the wild-type S is shown. To determine the relative level of S palmitoylation, all S protein species film images obtained by autoradiography were scanned, digitally analyzed, and normalized to the total protein of the sample obtained by spectrophotometry (not shown). The amount of palmitoylation was then expressed as a ratio to the relative amount of wild-type S.

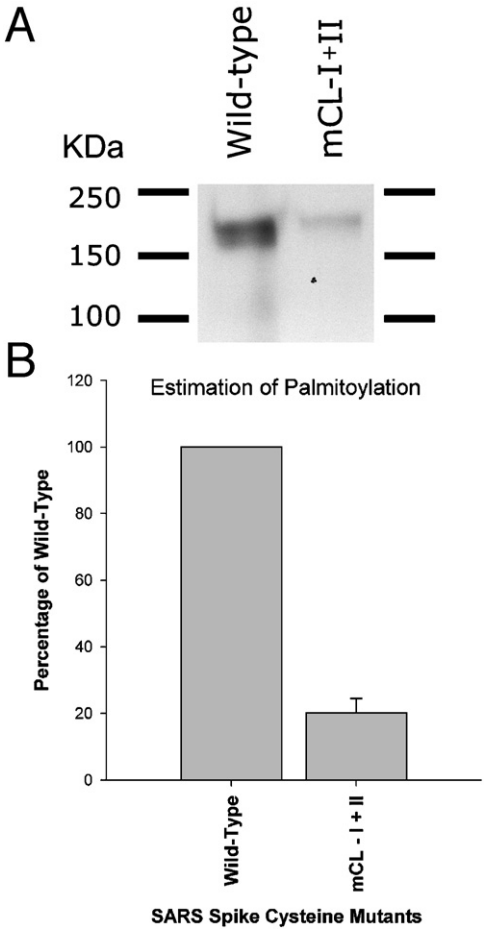

Fig. 7. Incorporation of [^{3}H] palmitic acid into wild-type and double cysteine mutant forms mCL-I+II of the SARS–CoV S glycoprotein. (A) Autoradiograms of immunoprecipitates as in Fig. 6A for the double-mutant mCL-I+II. (B) An estimation of the relative concentration of the palmitoylated S species in comparison to the wild-type S is shown as in Fig. 6B.

S-palmitoylation and S-mediated cell fusion

Wild-type S as well as mutant S glycoproteins were efficiently labeled with ^{3}H-palmitic acid indicating that the SARS–CoV S is palmitoylated. Analysis of the different S mutants revealed that the two cysteine clusters proximal to the TMD are major sites for S palmitoylation, since ^{3}H-palmitic acid incorporation was significantly reduced in the mCL-I and mCL-II cluster mutations. This conclusion is further supported by the fact that combination of the mCL-I and mCL-II mutations into S mutant form mCL-I+II reduced palmitoylation by more than 80% in comparison to the wild-type S. In contrast, the mCL-III and mCL-IV mutations did not drastically affect ^{3}H-palmitic acid incorporation into these S mutant glycoproteins indicating that these cysteine residues are probably not efficiently palmitoylated. The residual palmitoylation observed in the S mutant form mCL-I+II indicates that some of these other cysteine residues within the carboxyl terminus of the S glycoprotein may be inefficiently palmitoylated.

The mCL-I and mCL-II mutations drastically affected S-mediated cell fusion, while the mCL-III and mCL-IV mutations caused an approximate 15% reduction in cell fusion. The mCL-I+II mutation reduced S-mediated cell fusion to approximately the same level as the mCL-I and mCL-II mutations alone (not shown) indicating that palmitoylation of the S carboxyl terminus at the membrane proximal cysteine residues enhances S-mediated cell fusion, but it is not absolutely necessary for S-mediated cell fusion. Furthermore, none of the mutations including the double mutant mCL-I+II significantly affected the levels of S cell-surface expression. These results strongly suggest that palmitoylation of cysteine residues within the carboxyl terminus of S is important for S mediated cell fusion with the proximal to the TMD cysteines being primary sites for palmitoylation. Based on the low levels of reduction of S-mediated cell fusion by the S-mutant forms mCL-III and mCL-IV, as well as the low level of palmytoylation of the S-mutant form mCL-I+II, it is possible that the cysteine residues altered in the mCL-III and mCL-IV mutations are also inefficiently palmitoylated. This inefficient palmytoylation may help sustain basal fusogenic functions of S.

The carboxyl terminal cysteine residues of viral membrane glycoproteins have been reported to serve as potential palmitoylation sites (Ponimaskin and Schmidt, 1995; Rose et al., 1984; Schlesinger et al., 1993; Schmidt, 1989; Sefton and Buss, 1987). Palmitoylation of viral glycoproteins involved in cell fusion have been shown to affect the ability to fuse cellular membranes, virus infection of cells, and virus assembly (Glick and Rothman, 1987; Jin et al., 1996; Melikyan et al., 2000; Naim et al., 1992; Schroth-Diez et al., 1998; Zurcher et al., 1994). Specifically for coronaviruses, it has been shown that the S2 fragment of the MHV and the human coronavirus A59 S glycoprotein is palmitoylated on its carboxyl-terminal region (Niemann and Klenk, 1981; Sturman et al., 1980; van Berlo et al., 1987). Furthermore, the MHV S C1217 and C1223 amino acid residues have been shown to be potential acylation sites (Bos et al., 1995).

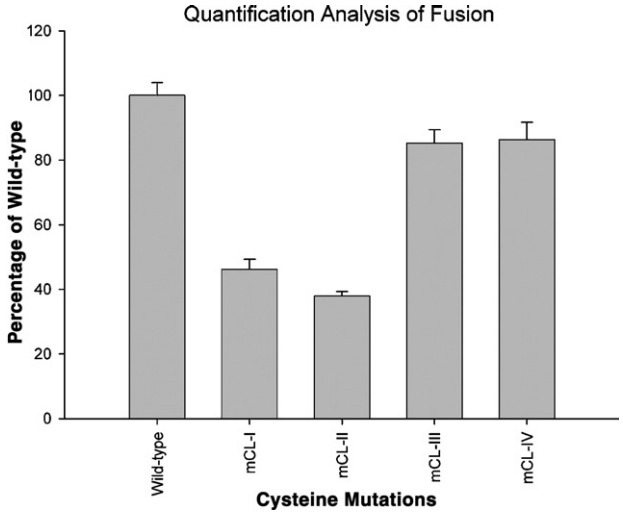

Fig. 8. Quantitation of the extent of S-mediated cell fusion. The average size of syncytia for each mutant was determined by digitally analyzing the area of approximately 300 syncytia stained by immunohistochemistry for S glycoprotein expression using the Image Pro Plus 5.0 software package (see Materials and methods). Error bars shown represent the standard deviation calculated through comparison of the data from each of three experiments.

In general, cysteines proximal to the inner leaflet of the plasma membrane in viral proteins often undergo palmitic acid attachment through a thioester bond onto cysteine residues (Ponimaskin and Schmidt, 1995; Rose et al., 1984; Schlesinger et al., 1993; Schmidt, 1989; Sefton and Buss, 1987). The findings that the carboxyl terminus portion of the SARS–CoV S glycoprotein is palmitoylated substantially strengthen our transmembrane prediction model that places the palmitoylated cysteine residues proximal, but not within the TMD. Apparently, palmitoylation of these cysteine residues is not necessary for plasma membrane transport and anchoring, since none of the mutations seemed to drastically affect intracellular transport and cell-surface expression. However, palmitoylation may provide additional anchoring during extracellular receptor binding and S-mediated cell fusion, which must produce substantial stresses on TMD anchoring. Alternatively, it is possible that cytoplasmic conformational changes mediated by palmitoylation and other modifications alter the ability of the extracellular portion of S to assume the proper conformation required for optimum cell fusion, implying a signal transduction mechanism between the intracellular and extracellular domains.

Materials and methods

Cells and S monoclonal antibody

African green monkey kidney (Vero) cells were obtained from the American Type Culture Collection (Rockville, MD). Cells were propagated and maintained in Dulbecco's modified Eagle medium (Sigma Chemical Co., St. Louis, MO) containing sodium bicarbonate and 15 mM HEPES supplemented with 10% heat-inactivated fetal bovine serum. The monoclonal antibodies SW-111 was raised against the Spike envelope glycoprotein of the SARS–CoV virus as described in detail previously (Petit et al., 2005).

Plasmids

The parental plasmid used in the present study, SARS-S-Optimized, has been previously described (Li et al., 2003). The Spike–3XFLAG–N gene construct was generated by cloning the codon-optimized S gene, without the DNA sequence coding for the signal peptide, into the p3XFLAG–CMV-9 plasmid vector (Sigma). PCR overlap extension (Aiyar et al., 1996) was used to construct the cluster to alanine mutants as described previously (Petit et al., 2005). Restriction endonuclease sites *Bam*HI and *Pml*I were then used to clone the gene construct into the Spike–3XFLAG–N plasmid. The constructed cluster mutants targeting the S cysteine-rich region changed the following sets of amino acids to alanine residues: mCL-I: C(1217), C(1218); mCL-II: C(1223), C (1224), C(1226); mCL-III: C(1230), C(1232); mCL-IV: C(1235), C(1236) (Fig. 2).

Western blot analysis

Vero cell monolayers in six-well plates were transfected with the indicated plasmids utilizing the Lipofectamine 2000 reagent (Invitrogen) according to the manufacturer's directions. At 48 h post-transfection, cells were collected by low-speed centrifugation, washed with Tris-buffered saline (TBS), and lysed on ice for 15 min in mammalian protein extraction reagent supplemented with a cocktail of protease inhibitors (Invitrogen/Life Technologies). Insoluble cell debris was pelleted, samples were electrophoretically separated by SDS–PAGE, transferred to nitrocellulose membranes, and probed with anti-SARS–CoV monoclonal antibody at a 1:10 dilution as described in detail previously (Petit et al., 2005).

Cell surface immunohistochemistry

Vero cell monolayers in six-well plates were transfected with the indicated plasmids utilizing the Lipofectamine 2000 reagent (Invitrogen) according to the manufacturer's directions. At 48 h post-transfection, the cells were washed with TBS-Ca/Mg and either fixed with iced cold methanol or left unfixed (live). Immunohistochemistry was performed by utilizing the Vector Laboratories Vectastain Elite ABC kit (Vector Laboratories, Burlingame, CA) essentially as described in the manufacturer's directions and described in detail previously (Petit et al., 2005).

Determination of cell-surface to total cell S glycoprotein expression

Vero cell monolayers in six-well plates were transfected with the indicated plasmids and processed for immunohistochemistry as described above with the exception that the ABTS Substrate Kit, 2, 2′-azino-bis(3-ethylbenzthiazoline-6-sulfonic acid) (Vector Laboratories) was used instead of the NovaRed substrate. After the substrate was allowed to develop for 30 min, 100 μl of the developed substrate was transferred, in triplicate, to a 96-well plate. The samples were then analyzed for color change at a wavelength of 405 nm. The absorbance reading from cell-surface labeling experiments obtained from live cells were divided by the total labeled absorbance readings obtained from fixed cells which was then normalized to the wild-type protein values. The measurements were then converted to percentages reflecting the ratio of S present on cell-surfaces versus the total S expressed in the transfected cells.

Quantitation of the extent of S-mediated cell fusion

Vero cell monolayers in six-well plates were transfected in triplicate with the indicated plasmids utilizing the Lipofectamine 2000 reagent (Invitrogen) according to the manufacturer's directions. Concurrently, Vero cell monolayers in six-well plates were transfected with the plasmid encoding the ACE2 receptor protein utilizing the Lipofectamine 2000 reagent (Invitrogen) according to the manufacturer's directions. At 24 h post-transfection, cells containing the mutant plasmids, the ACE2 receptor, and normal untransfected cells were washed with TBS-Ca/Mg, trypsinized, and overlayed in a single well of a six-well plate at a ratio of 2 ml (cells transfected with the ACE2 receptor) : 0.5 ml (cells transfected with the mutant) : 1.5 ml (untransfected cells). All of the cells transfected with ACE2

were pooled to ensure that every well had an equal amount of cells with receptor expressed on their surface. After incubation for 24 h, the cells were washed with TBS-Ca/Mg and fixed with ice cold methanol. Immunohistochemistry was performed by utilizing the Vector Laboratories Vectastain Elite ABC kit essentially as described in the manufacturer's directions. Briefly, cells were washed with TBS-Ca/Mg and incubated in TBS blocking buffer supplemented with normal horse serum at room temperature for 1 h. After blocking, cells were reacted with anti-FLAG antibody (1:500) in TBS blocking buffer for 3 h, washed four times with TBS-Ca/Mg, and incubated with biotinylated horse anti-mouse antibody. Excess antibody was removed by four washes with TBS-Ca/Mg and subsequently incubated with Vectastain Elite ABC reagent for 30 min. Finally, cells were washed three times with TBS-Ca/Mg, and reactions were developed with NovaRed substrate (Vector Laboratories) according to the manufacturer's directions. The average size of syncytia for each mutant was determined by analyzing the area of approximately 300 syncytia, from digital images, using the Image Pro Plus 5.0 software package. The averages were then converted to percentages of the average syncytia size of the wild-type SARS–CoV S. Error bars represent the standard deviations calculated through comparison of the data from each of three experiments.

Incorporation of [^{3}H] palmitic acid into wild-type and mutant forms of the SARS–CoV S glycoproteins

To detect palmitoylation of the S glycoprotein, VERO cells were transfected with the wild-type SARS–CoV optimized S (SARS So 3xF), mCL-I, mCL-II, mCL-III, mCL-IV, and a protein control labeled with a 3xFLAG carboxyl tag , which served as a negative control. At 48 h post-transfection, the proteins were metabolically labeled with [^{3}H] palmitic acid (400 μCi/T_{25} plate) for 2 h at 37 °C. The labeled cells were washed three times with cold PBS and solubilized in 1 ml of lysis buffer, TES (20 mM Tris–HCl [pH 7.5], 100 mM NaCl, 1 mM EDTA) containing 1% Triton X-100 and 2 mM phenylmethylsulfonyl fluoride. Nuclei were removed from the lysates by centrifugation at 16,100×*g* for 10 min at 4 °C. Immunoprecipitation was then performed on the lysates using EZview Red ANTI-FLAG M2 Affinity Gel (Sigma) by following the manufacturer's protocol. The samples were then electrophoretically separated by SDS–PAGE. The gel was then treated with Amplify Fluorographic Reagent (Amersham Biosciences) according to protocol, dried, and visualized by exposing X-ray film for a period of 3 days. The exposed film was then scanned and digitally processed using the Image Pro Plus 5.0 software package.

References

Abraham, S., Kienzle, T.E., Lapps, W., Brian, D.A., 1990. Deduced sequence of the bovine coronavirus spike protein and identification of the internal proteolytic cleavage site. Virology 176 (1), 296–301.

Aiyar, A., Xiang, Y., Leis, J., 1996. Site-directed mutagenesis using overlap extension PCR. Methods Mol. Biol. 57, 177–191.

Anand, K., Ziebuhr, J., Wadhwani, P., Mesters, J.R., Hilgenfeld, R., 2003. Coronavirus main proteinase (3CLpro) structure: basis for design of anti-SARS drugs. Science 300 (5626), 1763–1767.

Bagai, S., Lamb, R.A., 1996. Truncation of the COOH-terminal region of the paramyxovirus SV5 fusion protein leads to hemifusion but not complete fusion. J. Cell Biol. 135 (1), 73–84.

Baker, K.A., Dutch, R.E., Lamb, R.A., Jardetzky, T.S., 1999. Structural basis for paramyxovirus-mediated membrane fusion. Mol. Cell 3 (3), 309–319.

Binns, M.M., Boursnell, M.E., Cavanagh, D., Pappin, D.J., Brown, T.D., 1985. Cloning and sequencing of the gene encoding the spike protein of the coronavirus IBV. J. Gen. Virol. 66 (Pt 4), 719–726.

Bos, E.C., Heijnen, L., Luytjes, W., Spaan, W.J., 1995. Mutational analysis of the murine coronavirus spike protein: effect on cell-to-cell fusion. Virology 214 (2), 453–463.

Bos, E.C., Luytjes, W., Spaan, W.J., 1997. The function of the spike protein of mouse hepatitis virus strain A59 can be studied on virus-like particles: cleavage is not required for infectivity. J. Virol. 71 (12), 9427–9433.

Bosch, B.J., van der Zee, R., de Haan, C.A., Rottier, P.J., 2003. The coronavirus spike protein is a class I virus fusion protein: structural and functional characterization of the fusion core complex. J. Virol. 77 (16), 8801–8811.

Broer, R., Boson, B., Spaan, W., Cosset, F.L., Corver, J., 2006. Important role for the transmembrane domain of severe acute respiratory syndrome coronavirus spike protein during entry. J. Virol. 80 (3), 1302–1310.

Cavanagh, D., 1995. The Coronavirus Surface Glycoprotein. Plenum Press Inc., New York, NY.

Chang, K.W., Sheng, Y., Gombold, J.L., 2000. Coronavirus-induced membrane fusion requires the cysteine-rich domain in the spike protein. Virology 269 (1), 212–224.

de Groot, R.J., Luytjes, W., Horzinek, M.C., van der Zeijst, B.A., Spaan, W.J., Lenstra, J.A., 1987. Evidence for a coiled-coil structure in the spike proteins of coronaviruses. J. Mol. Biol. 196 (4), 963–966.

Delmas, B., Gelfi, J., L'Haridon, R., Vogel, L.K., Sjostrom, H., Noren, O., Laude, H., 1992. Aminopeptidase N is a major receptor for the enteropathogenic coronavirus TGEV. Nature 357 (6377), 417–420.

Drosten, C., Gunther, S., Preiser, W., van der Werf, S., Brodt, H.R., Becker, S., Rabenau, H., Panning, M., Kolesnikova, L., Fouchier, R.A., Berger, A., Burguiere, A.M., Cinatl, J., Eickmann, M., Escriou, N., Grywna, K., Kramme, S., Manuguerra, J.C., Muller, S., Rickerts, V., Sturmer, M., Vieth, S., Klenk, H.D., Osterhaus, A.D., Schmitz, H., Doerr, H.W., 2003. Identification of a novel coronavirus in patients with severe acute respiratory syndrome. N Engl. J. Med. 348 (20), 1967–1976.

Eckert, D.M., Kim, P.S., 2001. Mechanisms of viral membrane fusion and its inhibition. Annu. Rev. Biochem. 70, 777–810.

Gabuzda, D.H., Lever, A., Terwilliger, E., Sodroski, J., 1992. Effects of deletions in the cytoplasmic domain on biological functions of human immunodeficiency virus type 1 envelope glycoproteins. J. Virol. 66 (6), 3306–3315.

Glick, B.S., Rothman, J.E., 1987. Possible role for fatty acyl-coenzyme A in intracellular protein transport. Nature 326 (6110), 309–312.

Godeke, G.J., de Haan, C.A., Rossen, J.W., Vennema, H., Rottier, P.J., 2000. Assembly of spikes into coronavirus particles is mediated by the carboxy-terminal domain of the spike protein. J. Virol. 74 (3), 1566–1571.

Gombold, J.L., Hingley, S.T., Weiss, S.R., 1993. Fusion-defective mutants of mouse hepatitis virus A59 contain a mutation in the spike protein cleavage signal. J. Virol. 67 (8), 4504–4512.

Hirokawa, T., Boon-Chieng, S., Mitaku, S., 1998. SOSUI: classification and secondary structure prediction system for membrane proteins. Bioinformatics 14 (4), 378–379.

Holmes, K.V., 2003. SARS-associated coronavirus. N Engl. J. Med. 348 (20), 1948–1951.

Ingallinella, P., Bianchi, E., Finotto, M., Cantoni, G., Eckert, D.M., Supekar, V.M., Bruckmann, C., Carfi, A., Pessi, A., 2004. Structural characterization of the fusion-active complex of severe acute respiratory syndrome (SARS) coronavirus. Proc. Natl. Acad. Sci. U. S. A. 101 (23), 8709–8714.

Jin, H., Subbarao, K., Bagai, S., Leser, G.P., Murphy, B.R., Lamb, R.A., 1996. Palmitylation of the influenza virus hemagglutinin (H3) is not essential for virus assembly or infectivity. J. Virol. 70 (3), 1406–1414.

Kielian, M., 2006. Class II virus membrane fusion proteins. Virology 344 (1), 38–47.

Krokhin, O., Li, Y., Andonov, A., Feldmann, H., Flick, R., Jones, S., Stroeher, U., Bastien, N., Dasuri, K.V., Cheng, K., Simonsen, J.N., Perreault, H., Wilkins, J., Ens, W., Plummer, F., Standing, K.G., 2003. Mass spectrometric characterization of proteins from the SARS virus: a preliminary report. Mol. Cell. Proteomics 2 (5), 346–356.

Ksiazek, T.G., Erdman, D., Goldsmith, C.S., Zaki, S.R., Peret, T., Emery, S., Tong, S., Urbani, C., Comer, J.A., Lim, W., Rollin, P.E., Dowell, S.F., Ling, A.E., Humphrey, C.D., Shieh, W.J., Guarner, J., Paddock, C.D., Rota, P., Fields, B., DeRisi, J., Yang, J.Y., Cox, N., Hughes, J.M., LeDuc, J.W., Bellini, W.J., Anderson, L.J., 2003. A novel coronavirus associated with severe acute respiratory syndrome. N Engl. J. Med. 348 (20), 1953–1966.

Kunkel, F., Herrler, G., 1993. Structural and functional analysis of the surface protein of human coronavirus OC43. Virology 195 (1), 195–202.

Lescar, J., Roussel, A., Wien, M.W., Navaza, J., Fuller, S.D., Wengler, G., Rey, F.A., 2001. The Fusion glycoprotein shell of Semliki Forest virus: an icosahedral assembly primed for fusogenic activation at endosomal pH. Cell 105 (1), 137–148.

Li, W., Moore, M.J., Vasilieva, N., Sui, J., Wong, S.K., Berne, M.A., Somasundaran, M., Sullivan, J.L., Luzuriaga, K., Greenough, T.C., Choe, H., Farzan, M., 2003. Angiotensin-converting enzyme 2 is a functional receptor for the SARS coronavirus. Nature 426 (6965), 450–454.

Lontok, E., Corse, E., Machamer, C.E., 2004. Intracellular targeting signals contribute to localization of coronavirus spike proteins near the virus assembly site. J. Virol. 78 (11), 5913–5922.

Luytjes, W., Sturman, L.S., Bredenbeek, P.J., Charite, J., van der Zeijst, B.A., Horzinek, M.C., Spaan, W.J., 1987. Primary structure of the glycoprotein E2 of coronavirus MHV-A59 and identification of the trypsin cleavage site. Virology 161 (2), 479–487.

Marra, M.A., Jones, S.J., Astell, C.R., Holt, R.A., Brooks-Wilson, A., Butterfield, Y.S., Khattra, J., Asano, J.K., Barber, S.A., Chan, S.Y., Cloutier, A., Coughlin, S.M., Freeman, D., Girn, N., Griffith, O.L., Leach, S.R., Mayo, M., McDonald, H., Montgomery, S.B., Pandoh, P.K., Petrescu, A.S., Robertson, A.G., Schein, J.E., Siddiqui, A., Smailus, D.E., Stott, J.M., Yang, G.S., Plummer, F., Andonov, A., Artsob, H., Bastien, N., Bernard, K., Booth, T.F., Bowness, D., Czub, M., Drebot, M., Fernando, L., Flick, R., Garbutt, M., Gray, M., Grolla, A., Jones, S., Feldmann, H., Meyers, A., Kabani, A., Li, Y., Normand, S., Stroher, U., Tipples, G.A., Tyler, S., Vogrig, R., Ward, D., Watson, B., Brunham, R.C., Krajden, M., Petric, M., Skowronski, D.M., Upton, C., Roper, R.L., 2003. The Genome sequence of the SARS-associated coronavirus. Science 300 (5624), 1399–1404.

Melikyan, G.B., Markosyan, R.M., Hemmati, H., Delmedico, M.K., Lambert, D.M., Cohen, F.S., 2000. Evidence that the transition of HIV-1 gp41 into a six-helix bundle, not the bundle configuration, induces membrane fusion. J. Cell Biol. 151 (2), 413–423.

Mounir, S., Talbot, P.J., 1993. Molecular characterization of the S protein gene of human coronavirus OC43. J. Gen. Virol. 74 (Pt 9), 1981–1987.

Naim, H.Y., Amarneh, B., Ktistakis, N.T., Roth, M.G., 1992. Effects of altering palmitylation sites on biosynthesis and function of the influenza virus hemagglutinin. J. Virol. 66 (12), 7585–7588.

Niemann, H., Klenk, H.D., 1981. Coronavirus glycoprotein E_1, a new type of viral glycoprotein. J. Mol. Biol. 153 (4), 993–1010.

Parker, S.E., Gallagher, T.M., Buchmeier, M.J., 1989. Sequence analysis reveals extensive polymorphism and evidence of deletions within the E2 glycoprotein gene of several strains of murine hepatitis virus. Virology 173 (2), 664–673.

Peiris, J.S., Lai, S.T., Poon, L.L., Guan, Y., Yam, L.Y., Lim, W., Nicholls, J., Yee, W.K., Yan, W.W., Cheung, M.T., Cheng, V.C., Chan, K.H., Tsang, D.N., Yung, R.W., Ng, T.K., Yuen, K.Y., 2003. Coronavirus as a possible cause of severe acute respiratory syndrome. Lancet 361 (9366), 1319–1325.

Petit, C.M., Melancon, J.M., Chouljenko, V.N., Colgrove, R., Farzan, M., Knipe, D.M., Kousoulas, K.G., 2005. Genetic analysis of the SARS–coronavirus spike glycoprotein functional domains involved in cell-surface expression and cell-to-cell fusion. Virology 215–230.

Ponimaskin, E., Schmidt, M.F., 1995. Acylation of viral glycoproteins: structural requirements for palmitoylation of transmembrane proteins. Biochem. Soc. Trans. 23 (3), 565–568.

Raabe, T., Schelle-Prinz, B., Siddell, S.G., 1990. Nucleotide sequence of the gene encoding the spike glycoprotein of human coronavirus HCV 229E. J. Gen. Virol. 71 (Pt 5), 1065–1073.

Rasschaert, D., Laude, H., 1987. The predicted primary structure of the peplomer protein E2 of the porcine coronavirus transmissable gastroenteritis virus. J. Gen. Virol. 68 (Pt 7), 1883–1890.

Rose, J.K., Adams, G.A., Gallione, C.J., 1984. The presence of cysteine in the cytoplasmic domain of the vesicular stomatitis virus glycoprotein is required for palmitate addition. Proc. Natl. Acad. Sci. U. S. A. 81 (7), 2050–2054.

Rota, P.A., Oberste, M.S., Monroe, S.S., Nix, W.A., Campagnoli, R., Icenogle, J.P., Penaranda, S., Bankamp, B., Maher, K., Chen, M.H., Tong, S., Tamin, A., Lowe, L., Frace, M., DeRisi, J.L., Chen, Q., Wang, D., Erdman, D.D., Peret, T.C., Burns, C., Ksiazek, T.G., Rollin, P.E., Sanchez, A., Liffick, S., Holloway, B., Limor, J., McCaustland, K., Olsen-Rasmussen, M., Fouchier, R., Gunther, S., Osterhaus, A.D., Drosten, C., Pallansch, M.A., Anderson, L.J., Bellini, W.J., 2003. Characterization of a novel coronavirus associated with severe acute respiratory syndrome. Science 300 (5624), 1394–1399.

Russell, C.J., Jardetzky, T.S., Lamb, R.A., 2001. Membrane fusion machines of paramyxoviruses: capture of intermediates of fusion. EMBO J. 20 (15), 4024–4034.

Sainz Jr., B., Rausch, J.M., Gallaher, W.R., Garry, R.F., Wimley, W.C., 2005. Identification and characterization of the putative fusion peptide of the severe acute respiratory syndrome-associated coronavirus spike protein. J. Virol. 79 (11), 7195–7206.

Schlesinger, M.J., Veit, M., Schmidt, M.F., 1993. Palmitoylation of cellular and viral proteins. In: Schlesinger, M.J. (Ed.), Lipid Modification of Proteins. CRC Press, Boca Raton, FL, pp. 1–19.

Schmidt, M.F., 1989. Fatty acylation of proteins. Biochim. Biophys. Acta 988 (3), 411–426.

Schroth-Diez, B., Ponimaskin, E., Reverey, H., Schmidt, M.F., Herrmann, A., 1998. Fusion activity of transmembrane and cytoplasmic domain chimeras of the influenza virus glycoprotein hemagglutinin. J. Virol. 72 (1), 133–141.

Schwegmann-Wessels, C., Al-Falah, M., Escors, D., Wang, Z., Zimmer, G., Deng, H., Enjuanes, L., Naim, H.Y., Herrler, G., 2004. A novel sorting signal for intracellular localization is present in the S protein of a porcine coronavirus but absent from severe acute respiratory syndrome-associated coronavirus. J. Biol. Chem. 279 (42), 43661–43666.

Sefton, B.M., Buss, J.E., 1987. The covalent modification of eukaryotic proteins with lipid. J. Cell Biol. 104 (6), 1449–1453.

Sergel, T., Morrison, T.G., 1995. Mutations in the cytoplasmic domain of the fusion glycoprotein of Newcastle disease virus depress syncytia formation. Virology 210 (2), 264–272.

Seth, S., Vincent, A., Compans, R.W., 2003. Mutations in the cytoplasmic domain of a paramyxovirus fusion glycoprotein rescue syncytium formation and eliminate the hemagglutinin–neuraminidase protein requirement for membrane fusion. J. Virol. 77 (1), 167–178.

Skehel, J.J., Wiley, D.C., 1998. Coiled coils in both intracellular vesicle and viral membrane fusion. Cell 95 (7), 871–874.

Snijder, E.J., Bredenbeek, P.J., Dobbe, J.C., Thiel, V., Ziebuhr, J., Poon, L.L., Guan, Y., Rozanov, M., Spaan, W.J., Gorbalenya, A.E., 2003. Unique and conserved features of genome and proteome of SARS–coronavirus, an early split-off from the coronavirus group 2 lineage. J. Mol. Biol. 331 (5), 991–1004.

Song, H.C., Seo, M.Y., Stadler, K., Yoo, B.J., Choo, Q.L., Coates, S.R., Uematsu, Y., Harada, T., Greer, C.E., Polo, J.M., Pileri, P., Eickmann, M., Rappuoli, R., Abrignani, S., Houghton, M., Han, J.H., 2004. Synthesis and characterization of a native, oligomeric form of recombinant severe acute respiratory syndrome coronavirus spike glycoprotein. J. Virol. 78 (19), 10328–10335.

Stauber, R., Pfleiderera, M., Siddell, S., 1993. Proteolytic cleavage of the murine coronavirus surface glycoprotein is not required for fusion activity. J. Gen. Virol. 74 (Pt 2), 183–191.

Sturman, L.S., Holmes, K.V., Behnke, J., 1980. Isolation of coronavirus envelope glycoproteins and interaction with the viral nucleocapsid. J. Virol. 33 (1), 449–462.

Tong, S., Li, M., Vincent, A., Compans, R.W., Fritsch, E., Beier, R., Klenk, C., Ohuchi, M., Klenk, H.D., 2002. Regulation of fusion activity by the cytoplasmic domain of a paramyxovirus F protein. Virology 301 (2), 322–333.

Tsai, J.C., Zelus, B.D., Holmes, K.V., Weiss, S.R., 2003. The N-terminal domain of the murine coronavirus spike glycoprotein determines the CEACAM1 receptor specificity of the virus strain. J. Virol. 77 (2), 841–850.

van Berlo, M.F., van den Brink, W.J., Horzinek, M.C., van der Zeijst, B.A., 1987. Fatty acid acylation of viral proteins in murine hepatitis virus-infected cells. Brief report. Arch. Virol. 95 (1–2), 123–128.

Waning, D.L., Russell, C.J., Jardetzky, T.S., Lamb, R.A., 2004. Activation of a paramyxovirus fusion protein is modulated by inside-out signaling from the cytoplasmic tail. Proc. Natl. Acad. Sci. U. S. A. 101 (25), 9217–9222.

Wu, X.D., Shang, B., Yang, R.F., Yu, H., Ma, Z.H., Shen, X., Ji, Y.Y., Lin, Y., Wu, Y.D., Lin, G.M., Tian, L., Gan, X.Q., Yang, S., Jiang, W.H., Dai, E.H., Wang, X.Y., Jiang, H.L., Xie, Y.H., Zhu, X.L., Pei, G., Li, L., Wu, J.R., Sun, B., 2004. The spike protein of severe acute respiratory syndrome (SARS) is cleaved in virus infected Vero-E6 cells. Cell Res. 14 (5), 400–406.

Yao, Q., Compans, R.W., 1995. Differences in the role of the cytoplasmic domain of human parainfluenza virus fusion proteins. J. Virol. 69 (11), 7045–7053.

Ye, R., Montalto-Morrison, C., Masters, P.S., 2004. Genetic analysis of determinants for spike glycoprotein assembly into murine coronavirus virions: distinct roles for charge-rich and cysteine-rich regions of the endodomain. J. Virol. 78 (18), 9904–9917.

Ying, W., Hao, Y., Zhang, Y., Peng, W., Qin, E., Cai, Y., Wei, K., Wang, J., Chang, G., Sun, W., Dai, S., Li, X., Zhu, Y., Li, J., Wu, S., Guo, L., Dai, J., Wan, P., Chen, T., Du, C., Li, D., Wan, J., Kuai, X., Li, W., Shi, R., Wei, H., Cao, C., Yu, M., Liu, H., Dong, F., Wang, D., Zhang, X., Qian, X., Zhu, Q., He, F., 2004. Proteomic analysis on structural proteins of severe acute respiratory syndrome coronavirus. Proteomics 4 (2), 492–504.

Zelus, B.D., Schickli, J.H., Blau, D.M., Weiss, S.R., Holmes, K.V., 2003. Conformational changes in the spike glycoprotein of murine coronavirus are induced at 37 degrees C either by soluble murine CEACAM1 receptors or by pH 8. J. Virol. 77 (2), 830–840.

Zurcher, T., Luo, G., Palese, P., 1994. Mutations at palmitoylation sites of the influenza virus hemagglutinin affect virus formation. J. Virol. 68 (9), 5748–5754.